THE JOURNAL OF PHYSICAL CHEMISTRY Letters

pubs.acs.org/JPCL

Letter

Suppressing Molecular Charging, Nanochemistry, and Optical Rectification in the Tip-Enhanced Raman Geometry

Chih-Feng Wang, Brian T. O'Callahan, Dmitry Kurouski, Andrey Krayev, Zachary D. Schultz, and Patrick Z. El-Khoury*

Cite This: *J. Phys. Chem. Lett.* 2020, 11, 5890−5895

Read Online

ACCESS | Metrics & More | Article Recommendations | Supporting Information

ABSTRACT: Classical versus quantum plasmons are responsible for the recorded signals in non-contact-mode versus contact-mode tip-enhanced Raman spectroscopy (TERS) and lead to distinct observables. Under otherwise identical experimental conditions, we illustrate the concept through tapping- and contact-mode TERS mapping of chemically functionalized silver nanocubes. Whereas molecular charging, chemical transformations, and optical rectification are prominent observables in contact-mode TERS, the same effects are suppressed using tapping-mode feedback. In effect, this work demonstrates that nanoscale physical and chemical processes can be accessed and/or suppressed on demand in the TERS geometry. The advantages of tapping-mode TERS are otherwise highlighted with the latter in mind.

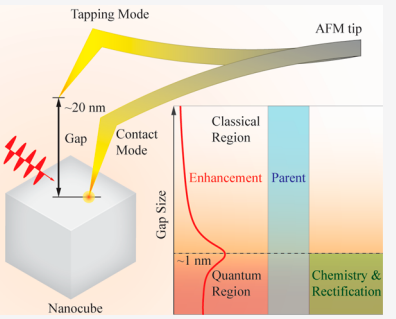

The combination of scanning probe microscopy and plasmon-enhanced Raman spectroscopy has enabled fingerprinting and imaging single molecules through tip-enhanced Raman scattering (TERS[1−3]).[4−7] In atomic force microscopy (AFM)-based two-dimensional (2D) TERS imaging measurements, a significant body of work that is documented in the literature takes advantage of plasmonic tip−sample nanojunctions to optimally localize and enhance the incident and scattered optical fields.[3,8,9] In this scheme, molecular/material systems that are interrogated through TERS are sandwiched between plasmonic tips and substrates. This geometry in many ways resembles prototypical plasmonic antennae, e.g., plasmonic dimers,[10] which have been previously used to detect and/or identify single molecules through variants of surface-enhanced Raman spectroscopy (SERS[11−14]).[15]

In recent investigations, we demonstrated that several physical and chemical phenomena contribute to molecular signals that are nascent from plasmonic tip−sample nanojunctions.[16−19] Pertinent to this work are prior demonstrations of molecular charging,[16−18,20] chemical transformations,[21] and optical rectification[17,18] in gap-mode TERS. In this regard, the quest for analytical/non-invasive TERS measurements is not well served: rather than imaging target molecules in a nonperturbative fashion, their anions[16−18,20] and (photo)-products[21−24] are formed throughout the course of TERS mapping as a mere consequence of the interplay between molecules and plasmons. After all, the same plasmons that enhance the optical cross sections of molecules in TERS[21−24] allegedly (more on this below) induce physical and chemical changes in them.[25]

Hybrid plasmonic eigenmodes of interacting plasmonic nanostructures have received extensive scrutiny in both theory and experiment.[26−32] It is now well-understood that plasmonic junctions that are <1 nm in size cannot be described using classical theories.[6,26−32] Indeed, nonlocal screening and electron tunneling are among the quantum mechanical effects that modify the lifetimes and resonances of junction plasmons. The general functional form that governs plasmonic field enhancement throughout the transition from bonding dipolar to charge-shuttling plasmons is somewhat well-established:[26−32] enhancement increases as the gap size decreases until the onset of nonclassicality (∼1 nm), where enhancement decreases with a further decrease in gap size, in part because of the nonlocal nature of charge-shuttling quantum plasmons. This is contrasted with the classical picture in which field enhancement only increases with a decrease in gap size.[26−32] Classically, the nature of the optical response (bonding dipolar resonance) is also unaltered as a function of gap size, whereas quantum and quantum-corrected descriptions of junction plasmons have identified transitions between bonding dipolar and charge transfer plasmons in the small gap size (<1 nm) limit.[26−32] Although these concepts are now well-appreciated in studies of interacting plasmonic metallic nanoparticles and nanostructures, they have received much less attention from

Received: June 16, 2020
Accepted: July 3, 2020
Published: July 3, 2020

https://dx.doi.org/10.1021/acs.jpclett.0c01413
J. Phys. Chem. Lett. 2020, 11, 5890−5895

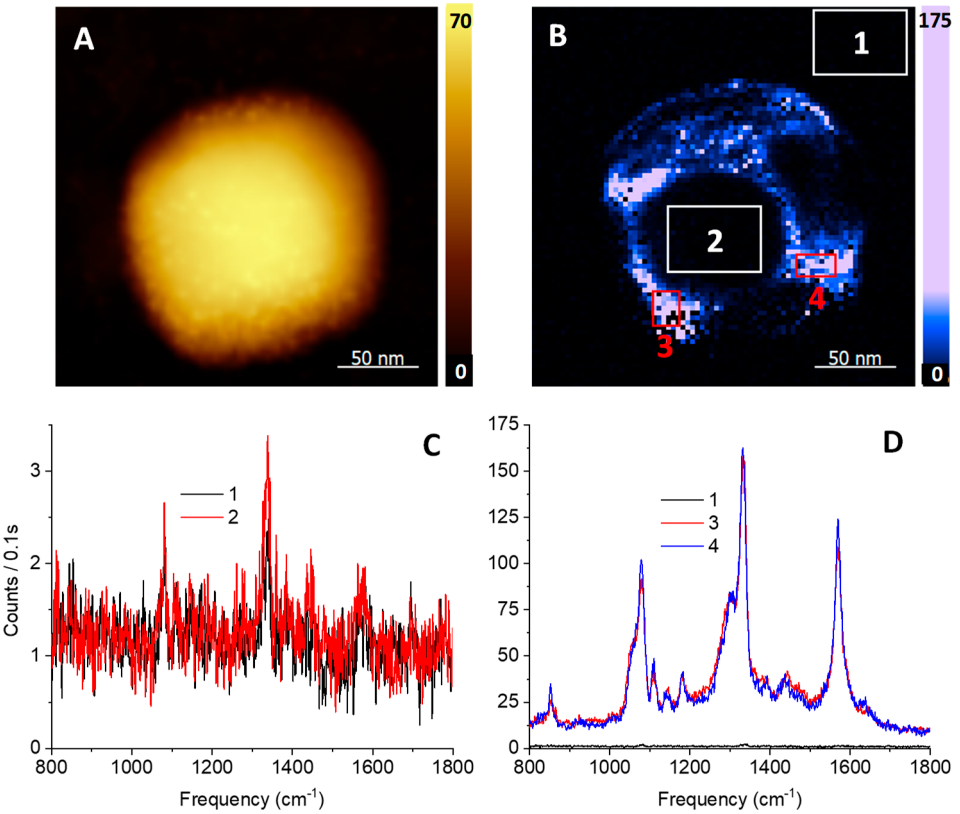

Figure 1. (A) AFM images recorded simultaneously with (B) contact-mode TERS images of a silver nanocube (~75 nm sides) coated with NTP. Shown in the ~1334 cm^{-1} TERS image. The resonance at this frequency corresponds to the symmetric NO_2 stretching of NTP. Several regions of interest are highlighted in panel B, and spatially averaged spectra contained within the designated areas are plotted in panels C (regions 1 and 2) and D (regions 1, 3, and 4). Parameters used in TERS: 50 $\mu W/\mu m^2$ at the sample position, 3 nm later step sizes, 0.1 s time integration/pixel.

the TERS community.[6,33−35] This is certainly the case in the context of AFM-based TERS, whereby tip−sample distance control is not trivial to achieve. With the definitions described above, contact-mode AFM-based gap-mode TERS must then be exclusively powered by nonclassical plasmons.[36,37] This is particularly the case for constructs in which ultrathin molecular layers define the size of the plasmonic gap between the probe and the underlying substrate. One of the goals of this work is to test the aforementioned premise.

In the TERS geometry, we previously associated background fluctuations in contact-mode TERS with charge transfer plasmons.[36,37] Both the nature of the molecular reporter[36,37] and the (contact- vs tapping-mode) feedback mechanism[38] that is used throughout the course of TERS measurements potentially comprise useful knobs for switching between classical/localized field-enhancing plasmons and nonlocal/quantum plasmons. Although the effects of different molecular linkers on the response at plasmonic nanojunctions have been revisited over the years,[39−41] how the feedback mechanism affects the observables in AFM-based TERS remains under-investigated, in part because of technical difficulties that are associated with tapping-mode TERS.[42,43] The latter is the subject of this study. Namely, we compare contact-mode versus tapping-mode TERS measurements primarily performed on 4-nitrothiophenol (NTP)- and 4-thiobenzonitrile (TBN)-functionalized silver nanocubes. We find that whereas effects such as plasmon-induced molecular charging, chemical transformations, and optical rectification are common occurrences in contact-mode TERS,[16−18] these phenomena are largely suppressed in tapping-mode TERS spectral images that were otherwise recorded under identical experimental conditions. We rationalize our observations with quantum descriptions of plasmonic nanojunctions in mind.

Correlated AFM contact-mode TERS images of a silver nanocube (75 nm) that is functionalized with NTP are shown in Figure 1. The TERS image shown is recorded using a hybrid feedback mechanism: spectra are recorded when the tip is in contact with the nanoparticle, whereas sample motion relative to the tip (pixel to pixel) is achieved using tapping-mode feedback. For the sake of simplicity, we refer to the latter as contact-mode TERS hereafter, as the spectra are recorded in contact mode. The contact-mode TERS image exhibits distinct high-intensity regions that trace the boundaries between the different faces of the cube. The response at the faces themselves is otherwise dim. This observation is reminiscent of prior TERS results from our group,[44] whereby the images of faceted plasmonic silver nanoparticles were brightest at facet boundaries that are characteristic of such particles. Consistent with our current observations, the response was also dim when the tip traced the facets.[44] Spectra taken in different regions of interest marked 1−4 in Figure 1B are plotted in panels C and D and further illustrate the concept. The off-particle (region 1) and on-face (region 2) spectra are comparable in their overall intensities. Significant contrast is observed between regions of high intensity (regions 3 and 4) on one hand and the dim on-face and off-particle spectra (regions 1 and 2) on the other. The dominant vibrational resonances of NTP at 1571, 1334, and 1079 cm^{-1} are immediately evident in Figure 1D.[16] Other peaks at 1435, 1389, ~1290, 1141, and ~1058 cm^{-1} are also observed. These peaks can be assigned to the dimercaptoazo-

https://dx.doi.org/10.1021/acs.jpclett.0c01413
J. Phys. Chem. Lett. 2020, 11, 5890−5895

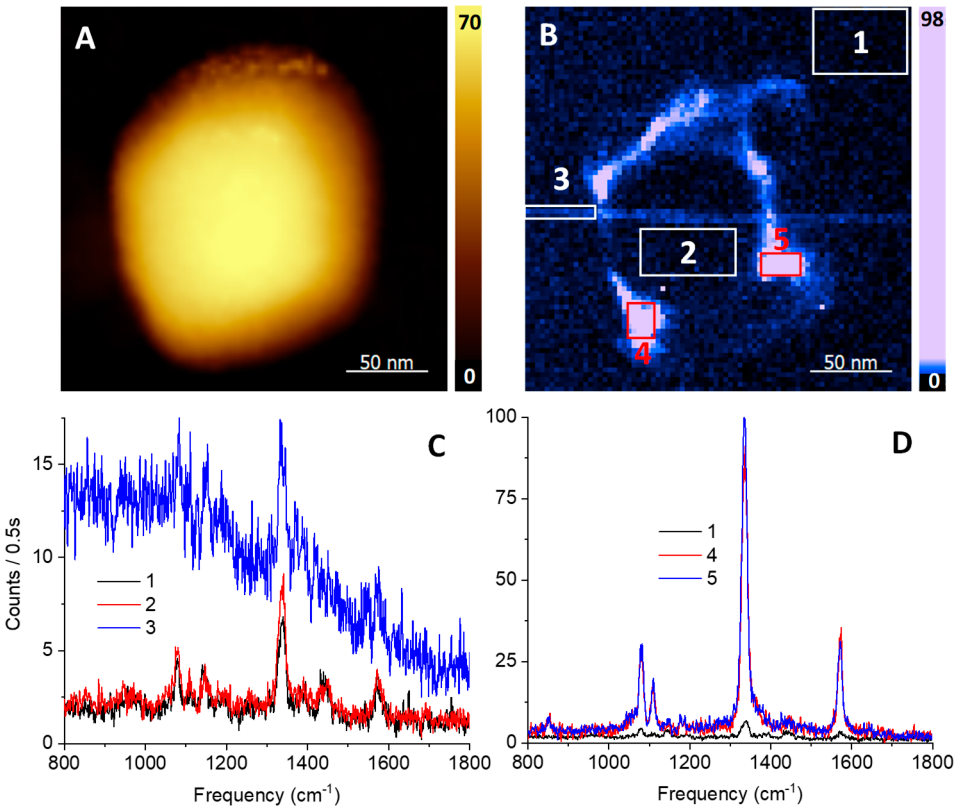

Figure 2. Combined (A) AFM and (B) tapping-mode TERS images of the same silver nanocube that is analyzed in Figure 1. The TERS map is again plotted at the symmetric NO_2 stretching vibrational resonance. Several regions are highlighted in panel B, and spatially averaged spectra contained within these regions are plotted in panels C (regions 1−3) and D (regions 1, 4, and 5). Parameters used in TERS: 50 $\mu W/\mu m^2$ at the sample position, 3 nm later step sizes, 0.5 s time integration/pixel.

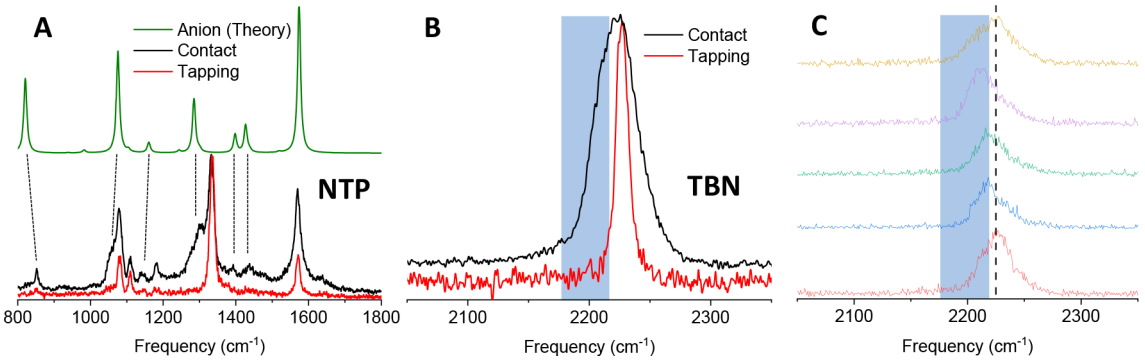

Figure 3. (A) Contact- and tapping-mode spectra taken from Figures 1D (region 4) and 2D (region 5) are compared to a theoretical spectrum of the anionic form of NTP (taken from ref 16). (B) Spatiotemporally averaged contact- and tapping-mode TERS spectra recorded from a TBN-coated silver nanocube. Several contact-mode TERS spectra are offset and compared in panel C. The dashed vertical line indicates the nominal frequency of the nitrile stretching vibration.

benzene (DMAB) product (1435, 1389, and 1141 cm^{-1})[21−23,45,46] and to an anionic form of NTP (a thiolate, which is marked by broad bands centered at ∼1290 and ∼1058 cm^{-1}), as elaborated in previous work.[16]

Correlated AFM tapping-mode TERS maps of the same NTP-functionalized silver nanocube that was analyzed in Figure 1 are shown in Figure 2. The contact- and tapping-mode TERS images are overall similar, with a few notable exceptions. First, sample drifting in the vertical direction throughout the course of the tapping-mode measurements is evident in both AFM and TERS images. This is due to the longer time integration used in this case (0.5 s/pixel). Second, a streak of dim but noticeable Raman activity is observed toward region 3 (see Figure 2B). This signal traces a 2−3 pixel-wide (6−9 nm) horizontal line, and its overall intensity is independent of the tip position. Noting that (i) the simultaneously recorded AFM map is unscathed in the same region of the image and (ii) the pre- and poststreak portions of the TERS image are similar in quality and resolution, we associate the observation with molecular transfer from the sample to the tip. More specifically, the observed signal is attributed to Raman scattering from tip-bound molecules. Nanoscale tip reconstruction throughout the course of TERS mapping cannot be rigorously ruled out; it is however less

https://dx.doi.org/10.1021/acs.jpclett.0c01413
J. Phys. Chem. Lett. 2020, 11, 5890−5895

likely given (ii) above and the fact that the TERS image in Figure 2B was recorded with tapping-mode feedback, which is generally less invasive than (intermittent) contact-mode TERS. At this juncture and on the basis of the spectra shown in panels C and D of Figures 1 and 2, it is useful to compare the differences between contact- and tapping-mode TERS signals that were recorded using the same tip and nanostructure. In contact (tapping) mode, the on/off particle contrast is 65 (15). After the disparate integration times (contact and tapping values of 0.1 and 0.5 s, respectively) are taken into account, the ratio of the brightest contact to tapping-mode signal is ∼8. This ratio is consistent with nominal residence times of the TERS probe within ∼1 nm of the surface: 10−20% of each oscillation period given a 20 nm peak-to-peak tapping amplitude.

Beyond the observed relative signal magnitudes, several aspects of the tapping- versus contact-mode TERS spectra are noteworthy. A side-to-side comparison of the spectra plotted in Figure 3A reveals that the former contains only the Raman signatures of NTP. The contact-mode spectrum on the other hand contains several additional peaks that can be assigned to an anionic NTP species and to the DMAB photoproduct, as described above. Repeating the measurements described thus far with TBN as a molecular reporter (Figure 3B,C) additionally illustrates that Stark-tuned vibrational resonances are observed in contact-mode TERS. A detailed analysis of the latter is documented elsewhere.[17,18] Tapping-mode TERS spectra on the other hand exclusively reveal a single sharp resonance at 2225 cm^{-1}, which corresponds to the (nominal) nitrile stretch in TBN. Minimally, the results obtained with NTP- and TBN-functionalized particles bolster the non-invasive nature of tapping-mode TERS mapping. Namely, chemical changes (charging and chemistry) and optical rectification, which are prominent observables in contact-mode TERS,[16−18,21] appear to be largely suppressed in tapping-mode TERS. The reproducibility and generality of these observations are ensured by performing similar measurements using different tips and substrates. Exemplary contact- versus tapping-mode TERS maps of a chemically functionalized Au nanocube attest to the latter (see the Supporting Information).

Classically, the same Raman signatures should be observed in tapping- and contact-mode TERS, the only difference being the relative signal magnitudes because of the shorter residence time of the TERS probe at the surface in tapping mode. This is not the case: we exclusively observe charging and optical rectification in contact-mode TERS (see Scheme 1). It is therefore tempting to deduce that under our experimental conditions, (i) quantum plasmons are exclusively responsible for molecular charging and chemical transformations and (ii) only tunneling (and not localized) plasmons are rectified. Naturally, the relative efficiencies of both processes depend on the exact experimental conditions, which we stress that herein besides the distinct feedback modes are otherwise identical throughout this work. In contrast, we observe a response that is consistent with classical junction plasmon-enhanced Raman scattering in tapping mode: enhanced NTP/TBN signatures are exclusively observed in this case. We therefore propose that localized plasmons that carry larger enhancement than their nonlocal/quantum analogues prior to the onset of tunneling (small gap distances) are sampled within the 20−40 nm tapping amplitude (∼300 kHz resonance frequency) of our probe and govern the time-integrated response at every pixel in tapping-mode TERS.

Scheme 1. Local Optical Field Properties as Inferred from Molecular Signatures in Contact- versus Tapping-Mode TERS[a]

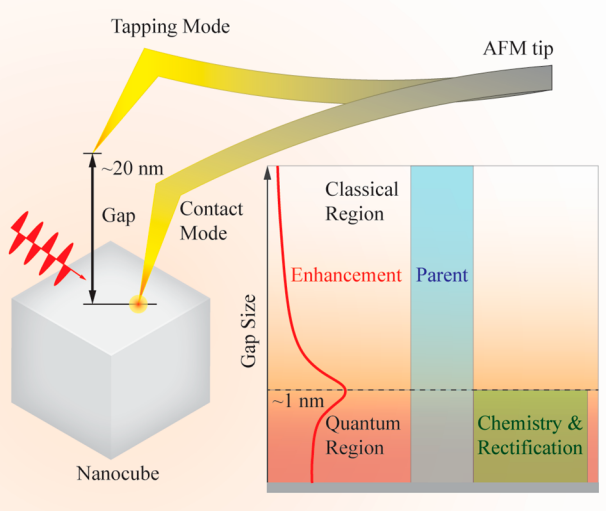

[a]See the text for more details.

The switch between contact-mode and tapping-mode feedback provides a mechanical perturbation analogous to the time-dependent changes in optical rectification noted by Nelson et al.[47] The previous study demonstrated that optically rectified surface potential was observed when plasmonic nanostructures were illuminated with CW illumination, but not with pulsed excitation. The 13 ns time window between pulses enabled short-lived plasmons to relax prior to the arrival of the next optical pulse. In this picture, the accumulation of charge derived from optical rectification occurs on a slower time scale. The lifetimes of optically induced plasmonic resonances are reported to be on the femto- to picosecond time scale,[48,49] and the resulting electric fields relax shortly after excitation.[50−52] In our context, it appears that charge is accumulated in contact mode, whereas tapping allows quantum plasmons to relax as the probe is distal from the surface, such that classical plasmons dominate the response.

It is important to point out that the images in both tapping- and contact-mode TERS still trace local fields that are excited under our present experimental conditions, as amply demonstrated in prior works from our group.[18,21,44,53,54] Non-contact-mode TERS mapping is however advantageous over its contact-mode analogue in that it is more analytical and less invasive in every sense. Namely, molecules are simply probed with high selectivity and sensitivity as opposed to charged and/or transformed as a mere consequence of TERS nanoimaging and nanospectroscopy. Moreover, molecules are not subjected to (often intense) rectified local fields in the non-contact-mode TERS configuration. Naturally, samples are also subjected to minimal mechanical forces that are characteristic of contact-mode feedback mechanisms. On the practical side, the lifetimes of TERS probes are also dramatically improved in tapping mode. That said, relatively longer integration times are required to obtain adequate signal-to-noise ratios in tapping-mode TERS because of the relatively short residence time of the probe in the region of high signal enhancement (prior to the onset of tunneling in our picture).

https://dx.doi.org/10.1021/acs.jpclett.0c01413
J. Phys. Chem. Lett. 2020, 11, 5890−5895

The latter may be restrictive from a 2D imaging perspective, particularly under ambient conditions, but should be adequate in nanospectroscopy/line imaging of (bio)molecular and material systems in various environments.

METHODS

A dilute (0.001%) solution of PAMAM (Sigma-Aldrich) in ethanol was deposited (spin-casted, 2000 rpm) on a silicon chip. Next, a 20 μL solution of silver nanocubes (75 nm, Sigma-Aldrich) was deposited onto the polymer-coated substrate. After the colloidal solution was air-dried, the substrate was rinsed with excess amounts of ethanol. Then, 20 μL solutions of NTP (3.8 mM) or TBN (1 mM) were deposited onto the substrate (silicon, thin layer of PAMAM, and 75 nm silver nanocubes bottom to top, respectively). The washing step (excess amounts of ethanol) was repeated prior to drying the sample with a stream of dry nitrogen.

Our combined AFM optical setup is described in previous publications from our group.[17,18,44] Briefly, silicon probes (Nanosensors, ATEC) sputtered with Au (100 nm thickness) were prepared and used for both topographic and nano-Raman measurements. Tapping-mode measurements were performed by scanning the sample with respect to an oscillating tip (20−40 nm amplitude, ∼300 kHz resonance frequency). Here, the driving laser source (633 nm, 50−75 μW) was focused onto the apex of the metal-coated AFM probe at a grazing angle (∼65°) with respect to the surface normal. The objective used to deliver and collect the incident and scattered radiation consists of a 100× air objective (Mitutoyo, 0.7 NA). The laser polarization was set using a half-waveplate, such that it coincides with the long axis of the tip. The backscattered radiation was filtered through several optical filters (dichroic, notch, and long pass) and registered using a fiber-coupled detection system that consists of a spectrometer (Andor, Shamrock 500) coupled to an EMCCD camera (Andor, Newton).

ASSOCIATED CONTENT

Supporting Information

The Supporting Information is available free of charge at https://pubs.acs.org/doi/10.1021/acs.jpclett.0c01413.

Contact- versus tapping-mode TERS images of NTP-functionalized Au nanocubes and TERS cross-sectional cut demonstrating pixel-limited (<3 nm) spatial resolution (PDF)

AUTHOR INFORMATION

Corresponding Author

Patrick Z. El-Khoury − *Physical Sciences Division, Pacific Northwest National Laboratory, Richland, Washington 99352, United States;* orcid.org/0000-0002-6032-9006; Email: patrick.elkhoury@pnnl.gov

Authors

Chih-Feng Wang − *Physical Sciences Division, Pacific Northwest National Laboratory, Richland, Washington 99352, United States;* orcid.org/0000-0002-3085-6614

Brian T. O'Callahan − *Earth and Biological Sciences Division, Pacific Northwest National Laboratory, Richland, Washington 99352, United States;* orcid.org/0000-0001-9835-3207

Dmitry Kurouski − *Department of Biochemistry and Biophysics, Texas A&M University, College Station, Texas 77843, United States;* orcid.org/0000-0002-6040-4213

Andrey Krayev − *Horiba Instruments Inc., Novato, California 94949, United States*

Zachary D. Schultz − *Department of Chemistry and Biochemistry, The Ohio State University, Columbus, Ohio 43210, United States;* orcid.org/0000-0003-1741-8801

Complete contact information is available at: https://pubs.acs.org/10.1021/acs.jpclett.0c01413

Notes

The authors declare no competing financial interest.

ACKNOWLEDGMENTS

This work was supported by the U.S. Department of Energy (DOE), Office of Science, Office of Basic Energy Sciences, Division of Chemical Sciences, Geosciences & Biosciences.

REFERENCES

(1) Anderson, M. S. Locally Enhanced Raman Spectroscopy with an Atomic Force Microscope. *Appl. Phys. Lett.* **2000**, *76*, 3130−3132.

(2) Stockle, R. M.; Suh, Y. D.; Deckert, V.; Zenobi, R. Nanoscale Chemical Analysis by Tip-Enhanced Locally Enhanced Raman Spectroscopy with an Atomic Force Microscope Raman Spectroscopy. *Chem. Phys. Lett.* **2000**, *318*, 131−136.

(3) Pettinger, B.; Schambach, P.; Villagómez, C. J.; Scott, N. Tip-Enhanced Raman Spectroscopy: Near-Fields Acting on a Few Molecules. *Annu. Rev. Phys. Chem.* **2012**, *63*, 379−399.

(4) He, Z.; Han, Z. H.; Kizer, M.; Linhardt, R. J.; Wang, X.; Sinyukov, A. M.; Wang, J. Z.; Deckert, V.; Sokolov, A. V.; Hu, J.; Scully, M. O. Tip-Enhanced Raman Imaging of Single-Stranded DNA with Single Base Resolution. *J. Am. Chem. Soc.* **2019**, *141*, 753−757.

(5) Zhang, R.; Zhang, Y.; Dong, Z. C.; Jiang, S.; Zhang, C.; Chen, L. G.; Zhang, L.; Liao, Y.; Aizpurua, J.; Luo, Y.; Yang, J. L.; Hou, J. G. Chemical mapping of a single molecule by plasmon-enhanced Raman scattering. *Nature* **2013**, *498*, 82−86.

(6) Lee, J.; Crampton, K. T.; Tallarida, N.; Apkarian, V. A. Visualizing vibrational normal modes of a single molecule with atomically confined light. *Nature* **2019**, *568*, 78−82.

(7) Pozzi, E. K.; Goubert, G.; Chiang, N. H.; Jiang, N.; Chapman, C. T.; McAnally, M. O.; Henry, A. I.; Seideman, T.; Schatz, G. C.; Hersam, M. C.; van Duyne, R. P. Ultrahigh-Vacuum Tip-Enhanced Raman Spectroscopy. *Chem. Rev.* **2017**, *117*, 4961−4982.

(8) Deckert-Gaudig, T.; Taguchi, A.; Kawata, S.; Deckert, V. Tip-Enhanced Raman Spectroscopy - From Early Developments to Recent Advances. *Chem. Soc. Rev.* **2017**, *46*, 4077−4110.

(9) Richard-Lacroix, M.; Zhang, Y.; Dong, Z. C.; Deckert, V. Mastering High Resolution Tip-Enhanced Raman Spectroscopy: Towards a Shift of Perception. *Chem. Soc. Rev.* **2017**, *46*, 3922−3944.

(10) Whitmore, D. D.; El-Khoury, P. Z.; Fabris, L.; Chu, P.; Bazan, G. C.; Potma, E. O.; Apkarian, V. A. High Sensitivity Surface-Enhanced Raman Scattering in Solution Using Engineered Silver Nanosphere Dimers. *J. Phys. Chem. C* **2011**, *115*, 15900−15907.

(11) Fleischmann, M.; Hendra, P. J.; McQuillan, A. J. Raman-Spectra of Pyridine Adsorbed at a Silver Electrode. *Chem. Phys. Lett.* **1974**, *26*, 163−166.

(12) Jeanmaire, D. L.; Vanduyne, R. P. Surface Raman Spectroelectrochemistry 0.1. Heterocyclic, Aromatic, and Aliphatic-Amines Adsorbed on Anodized Silver Electrode. *J. Electroanal. Chem. Interfacial Electrochem.* **1977**, *84*, 1−20.

(13) Moskovits, M. Surface-Roughness and Enhanced Intensity of Raman-Scattering by Molecules Adsorbed on Metals. *J. Chem. Phys.* **1978**, *69*, 4159−4161.

(14) Otto, A. Raman-Spectra of CN^- Adsorbed at a Silver Surface. *Surf. Sci.* **1978**, *75*, L392−L396.

(15) El-Khoury, P. Z.; Abellan, P.; Chantry, R. L.; Gong, Y.; Joly, A. G.; Novikova, I. V.; Evans, J. E.; Apra, E.; Hu, D.; Ramasse, Q. M.; Hess, W. P. The Information Content in Single-Molecule Raman Nanoscopy. *Adv. Phys. X* **2016**, *1*, 35−54.
(16) Wang, R.; Li, J. B.; Rigor, J.; Large, N.; El-Khoury, P. Z.; Rogachev, A. Y.; Kurouski, D. Direct Experimental Evidence of Hot Carrier-Driven Chemical Processes in Tip-Enhanced Raman Spectroscopy (TERS). *J. Phys. Chem. C* **2020**, *124*, 2238−2244.
(17) Bhattarai, A.; Crampton, K. T.; Joly, A. G.; Wang, C. F.; Schultz, Z. D.; El-Khoury, P. Z. A Closer Look at Corrugated Au Tips. *J. Phys. Chem. Lett.* **2020**, *11*, 1915−1920.
(18) Bhattarai, A.; Cheng, Z.; Joly, A. G.; Novikova, I. V.; Evans, J. E.; Schultz, Z. D.; Jones, M. R.; El-Khoury, P. Z. Tip-Enhanced Raman Nanospectroscopy of Smooth Spherical Gold Nanoparticles. *J. Phys. Chem. Lett.* **2020**, *11*, 1795−1801.
(19) Wang, C. F.; Cheng, Z.; O'Callahan, B. T.; Crampton, K. T.; Jones, M. R.; El-Khoury, P. Z. Tip-Enhanced Multipolar Raman Scattering. *J. Phys. Chem. Lett.* **2020**, *11*, 2464−2469.
(20) Bhattarai, A.; El-Khoury, P. Z. Imaging Localized Electric Fields with Nanometer Precision through Tip-Enhanced Raman Scattering. *Chem. Commun.* **2017**, *53*, 7310−7313.
(21) Bhattarai, A.; El-Khoury, P. Z. Nanoscale Chemical Reaction Imaging at the Solid−Liquid Interface via TERS. *J. Phys. Chem. Lett.* **2019**, *10*, 2817−2822.
(22) Sun, J. J.; Su, H. S.; Yue, H. L.; Huang, S. C.; Huang, T. X.; Hu, S.; Sartin, M. M.; Cheng, J.; Ren, B. Role of Adsorption Orientation in Surface Plasmon-Driven Coupling Reactions Studied by Tip-Enhanced Raman Spectroscopy. *J. Phys. Chem. Lett.* **2019**, *10*, 2306−2312.
(23) Kumar, N.; Su, W. T.; Vesely, M.; Weckhuysen, B. M.; Pollard, A. J.; Wain, A. J. Nanoscale chemical imaging of solid-liquid interfaces using tip-enhanced Raman spectroscopy. *Nanoscale* **2018**, *10*, 1815−1824.
(24) van Schrojenstein Lantman, E. M.; Deckert-Gaudig, T.; Mank, A. J. G.; Deckert, V.; Weckhuysen, B. M. Catalytic Processes Monitored at the Nanoscale with Tip-Enhanced Raman Spectroscopy. *Nat. Nanotechnol.* **2012**, *7*, 583−586.
(25) Zhan, C.; Chen, X. J.; Yi, J.; Li, J. F.; Wu, D. Y.; Tian, Z. Q. From Plasmon-Enhanced Molecular Spectroscopy to Plasmon-Mediated Chemical Reactions. *Nat. Rev. Chem.* **2018**, *2*, 216−230.
(26) Zhu, W.; Esteban, R.; Borisov, A. G.; Baumberg, J. J.; Nordlander, P.; Lezec, H. J.; Aizpurua, J.; Crozier, K. B. Quantum Mechanical Effects in Plasmonic Structures with Subnanometre Gaps. *Nat. Commun.* **2016**, *7*, 11495.
(27) Nordlander, P. Molecular Tuning of Quantum Plasmon Resonances. *Science* **2014**, *343*, 1444−1445.
(28) Marinica, D. C.; Kazansky, A. K.; Nordlander, P.; Aizpurua, J.; Borisov, A. G. Quantum Plasmonics: Nonlinear Effects in the Field Enhancement of a Plasmonic Nanoparticle Dimer. *Nano Lett.* **2012**, *12*, 1333−9.
(29) Esteban, R.; Borisov, A. G.; Nordlander, P.; Aizpurua, J. Bridging Quantum and Classical Plasmonics with a Quantum-Corrected Model. *Nat. Commun.* **2012**, *3*, 825.
(30) Halas, N. J.; Lal, S.; Chang, W. S.; Link, S.; Nordlander, P. Plasmons in Strongly Coupled Metallic Nanostructures. *Chem. Rev.* **2011**, *111*, 3913−3961.
(31) Pérez-González, O.; Zabala, N.; Borisov, A.; Halas, N.; Nordlander, P.; Aizpurua, J. Optical Spectroscopy of Conductive Junctions in Plasmonic Cavities. *Nano Lett.* **2010**, *10*, 3090−3095.
(32) Savage, K. J.; Hawkeye, M. M.; Esteban, R.; Borisov, A. G.; Aizpurua, J.; Baumberg, J. J. Revealing the Quantum Regime in Tunnelling Plasmonics. *Nature* **2012**, *491*, 574−7.
(33) Zhang, Y.; Voronine, D. V.; Qiu, S.; Sinyukov, A. M.; Hamilton, M.; Liege, Z.; Sokolov, A. V.; Zhang, Z.; Scully, M. O. Improving Resolution in Quantum Subnanometre-Gap Tip-Enhanced Raman Nanoimaging. *Sci. Rep.* **2016**, *6*, 25788.
(34) Kravtsov, V.; Berweger, S.; Atkin, J. M.; Raschke, M. B. Control of Plasmon Emission and Dynamics at the Transition from Classical to Quantum Coupling. *Nano Lett.* **2014**, *14*, 5270−5.
(35) Liu, S. Y.; Muller, M.; Sun, Y.; Hamada, I.; Hammud, A.; Wolf, M.; Kumagai, T. Resolving the Correlation between Tip-Enhanced Resonance Raman Scattering and Local Electronic States with 1 nm Resolution. *Nano Lett.* **2019**, *19*, 5725−5731.
(36) El-Khoury, P. Z.; Hu, D. H.; Apkarian, V. A.; Hess, W. P. Raman Scattering at Plasmonic Junctions Shorted by Conductive Molecular Bridges. *Nano Lett.* **2013**, *13*, 1858−1861.
(37) El-Khoury, P. Z.; Hess, W. P. Vibronic Raman Scattering at the Quantum Limit of Plasmons. *Nano Lett.* **2014**, *14*, 4114−4118.
(38) El-Khoury, P. Z.; Hu, D. H.; Hess, W. P. Junction Plasmon-Induced Molecular Reorientation. *J. Phys. Chem. Lett.* **2013**, *4*, 3435−3439.
(39) Benz, F.; Tserkezis, C.; Herrmann, L. O.; de Nijs, B.; Sanders, A.; Sigle, D. O.; Pukenas, L.; Evans, S. D.; Aizpurua, J.; Baumberg, J. J. Nanooptics of Molecular-Shunted Plasmonic Nanojunctions. *Nano Lett.* **2015**, *15*, 669−674.
(40) Tan, S. F.; Wu, L.; Yang, J. K. W.; Bai, P.; Bosman, M.; Nijhuis, C. A. Quantum Plasmon Resonances Controlled by Molecular Tunnel Junctions. *Science* **2014**, *343*, 1496−1499.
(41) de Nijs, B.; Benz, F.; Barrow, S. J.; Sigle, D. O.; Chikkaraddy, R.; Palma, A.; Carnegie, C.; Kamp, M.; Sundararaman, R.; Narang, P.; Scherman, O. A.; Baumberg, J. J. Plasmonic Tunnel Junctions for Single-Molecule Redox Chemistry. *Nat. Commun.* **2017**, *8*, 994.
(42) Yu, J.; Saito, Y.; Ichimura, T.; Kawata, S.; Verma, P. Far-Field Free Tapping-Mode Tip-Enhanced Raman Microscopy. *Appl. Phys. Lett.* **2013**, *102*, 123110.
(43) Yano, T. A.; Ichimura, T.; Taguchi, A.; Hayazawa, N.; Verma, P.; Inouye, Y.; Kawata, S. Confinement of Enhanced Field Investigated by Tip-Sample Gap Regulation in Tapping-Mode Tip-Enhanced Raman Microscopy. *Appl. Phys. Lett.* **2007**, *91*, 121101.
(44) Bhattarai, A.; Novikova, I. V.; El-Khoury, P. Z. Tip-Enhanced Raman Nanographs of Plasmonic Silver Nanoparticles. *J. Phys. Chem. C* **2019**, *123*, 27765−27769.
(45) Zhao, L. B.; Chen, J. L.; Zhang, M.; Wu, D. Y.; Tian, Z. Q. Theoretical Study on Electroreduction of p-Nitrothiophenol on Silver and Gold Electrode Surfaces. *J. Phys. Chem. C* **2015**, *119*, 4949−4958.
(46) Huang, Y. F.; Zhu, H. P.; Liu, G. K.; Wu, D. Y.; Ren, B.; Tian, Z. Q. When the Signal Is Not from the Original Molecule To Be Detected: Chemical Transformation of para-Aminothiophenol on Ag during the SERS Measurement. *J. Am. Chem. Soc.* **2010**, *132*, 9244−9246.
(47) Nelson, D. A.; Schultz, Z. D. Impact of Plasmon-Induced Optically Rectified Electric Fields on Second Harmonic Generation. *J. Phys. Chem. C* **2019**, *123*, 20639−20648.
(48) Hartland, G. V. Optical Studies of Dynamics in Noble Metal Nanostructures. *Chem. Rev.* **2011**, *111*, 3858−3887.
(49) Brown, A. M.; Sundararaman, R.; Narang, P.; Goddard, W. A.; Atwater, H. A. Nonradiative Plasmon Decay and Hot Carrier Dynamics: Effects of Phonons, Surfaces, and Geometry. *ACS Nano* **2016**, *10*, 957−966.
(50) Aguirregabiria, G.; Marinica, D. C.; Esteban, R.; Kazansky, A. K.; Aizpurua, J.; Borisov, A. G. Role of Electron Tunneling in the Nonlinear Response of Plasmonic Nanogaps. *Phys. Rev. B: Condens. Matter Mater. Phys.* **2018**, *97*, 115430.
(51) Aguirregabiria, G.; Marinica, D. C.; Ludwig, M.; Brida, D.; Leitenstorfer, A.; Aizpurua, J.; Borisov, A. G. Dynamics of Electron-Emission Currents in Plasmonic Gaps Induced by Strong Fields. *Faraday Discuss.* **2019**, *214*, 147−157.
(52) Rybka, T.; Ludwig, M.; Schmalz, M. F.; Knittel, V.; Brida, D.; Leitenstorfer, A. Sub-Cycle Optical Phase Control of Nanotunnelling in the Single-Electron Regime. *Nat. Photonics* **2016**, *10*, 667−670.
(53) Bhattarai, A.; Crampton, K. T.; Joly, A. G.; Kovarik, L.; Hess, W. P.; El-Khoury, P. Z. Imaging the Optical Fields of Functionalized Silver Nanowires through Molecular TERS. *J. Phys. Chem. Lett.* **2018**, *9*, 7105−7109.
(54) Bhattarai, A.; Joly, A. G.; Hess, W. P.; El-Khoury, P. Z. Visualizing Electric Fields at Au(111) Step Edges via Tip-Enhanced Raman Scattering. *Nano Lett.* **2017**, *17*, 7131−7137.

https://dx.doi.org/10.1021/acs.jpclett.0c01413
J. Phys. Chem. Lett. 2020, 11, 5890−5895